中国光学（中英文） Chinese Optics 核心期刊

高性能中波红外陷波滤光片设计与研制

尚鹏 陈蓓曦 孙鹏 刘华松 白金林 季一勤 曹波 马远飞 林泉

Theoretical design and preparation of high performance MWiR notch filter

SHANG Peng, CHEN Bei-xi, SUN Peng, LIU Hua-song, BAI Jin-lin, JI Yi-qin, CAO Bo, MA Yuan-fei, LIN Quan

引用本文:
尚鹏, 陈蓓曦, 孙鹏, 刘华松, 白金林, 季一勤, 曹波, 马远飞, 林泉. 高性能中波红外陷波滤光片设计与研制[J]. 中国光学, 2023, 16(4): 904–915. doi: 10.37188/CO.2022–0193
SHANG Peng, CHEN Bei-xi, SUN Peng, LIU Hua-song, BAI Jin-lin, JI Yi-qin, CAO Bo, MA Yuan-fei, LIN Quan. Theoretical design and preparation of high performance MWiR notch filter[J]. *Chinese Optics*, 2023, 16(4): 904-915. doi: 10.37188/CO.2022-0193

在线阅读 View online: https://doi.org/10.37188/CO.2022–0193

文章编号 2097-1842(2023)04-0904-12

Theoretical design and preparation of high performance MWiR notch filter

SHANG Peng[1,2], CHEN Bei-xi[3], SUN Peng[2], LIU Hua-song[2*], BAI Jin-lin[2], JI Yi-qin[2], CAO Bo[1*], MA Yuan-fei[1], LIN Quan[1]

(1. *GRINM Guojing Advanced Materials Co., Ltd, General Research Institute for Nonferrous Metals, Beijing* 100088, *China*;
2. *Tianjin Key Laboratory of Optical Thin Film, Tianjin Jinhang Technical Physics Institute, Tianjin* 300308, *China*;
3. *Northwestern Polytechnical University, Xi'an* 710129, *China*)

* *Corresponding author, E-mail: liuhuasong@hotmail.com; caobo@guojing-tech.com*

Abstract: In order to effectively suppress the interference of CO_2 radiation 4.3 μm on MWiR target signal with wavelength of 3 μm−5 μm, based on the Needle random intercalation optimization algorithm, an accurate inversion correction model for the growth error of multi-layer ultra-thick Ge/Al_2O_3 films under quartz crystal monitoring is established by the electron beam evaporation method, thus realizing the design, the accurate inversion and the accurate preparation of MWiR notch filter. In order to solve the problem that the surface profile of the MWiR notch filter changes greatly, the preset substrate surface method is used to realize the low surface profile regulation of MWiR notch filter. The results show that the high refractive index Ge film has good deposition stability with the increase of coating time, while the deposition scale factor of low refractive index Al_2O_3 thin film changes up to 11.9% in a regular gradual trend. For the prepared MWiR notch filter, the average cut-off transmittance is less than 0.3% in the wavelength range of 4.2 μm−4.5 μm, and the average transmittances are more than 95% in the wavelength range of 3.5 μm−4.05 μm and 4.7 μm−5.0 μm. The surface profile of the substrate after coating can be effectively controlled in a small range. The film has good adaptability to complex environment, and has successfully passed the environmental test of firmness, high temperature, low temperature and damp heat specified in GJB 2485-95.

Key words: electron beam evaporation; quartz crystal deposition monitor; infrared filter; thin film; inversion correction

收稿日期:2022-09-16; **修订日期**:2022-10-08

基金项目:国家自然科学基金(No. 61905179);河北省自然科学基金(No. F2022103002);河北省重点研发计划项目(No. 22351101D)

Supported by the National Natural Science Foundation of China (No. 61905179); Natural Science Foundation of Hebei Province (No. F2022103002); Key R & D Projects of Hebei Province (No. 22351101D)

高性能中波红外陷波滤光片设计与研制

尚　鹏[1,2], 陈蓓曦[3], 孙　鹏[2], 刘华松[2*], 白金林[2], 季一勤[2], 曹　波[1*], 马远飞[1], 林　泉[1]
（1. 有研国晶辉新材料有限公司北京有色金属研究总院, 北京 100088;
2. 天津津航技术物理研究所 天津市薄膜光学重点实验室, 天津 300308;
3. 西北工业大学, 陕西 西安 710129）

摘要: 为了有效抑制 4.3 μm CO_2 辐射对 3 μm~5 μm 中波红外目标信号的干扰, 基于 Needle 随机插层优化算法, 采用电子束蒸发方法, 建立了石英晶振监控方式下多层超厚 Ge/Al_2O_3 薄膜生长误差的精确反演修正模型, 实现了中波红外陷波滤光片的设计、精确反演与制备; 同时, 针对中波红外陷波滤光片存在的面型变化大的问题, 采用预置基底面型方法, 实现了中波红外陷波滤光片低面型调控。研究结果表明: 随着镀膜时间的增加, 高折射率 Ge 膜具有较好的生长稳定性, 而低折射率 Al_2O_3 薄膜材料沉积比例因子变化高达 11.9%, 且呈规律性渐变趋势; 所制备的中波红外陷波滤光片在 4.2 μm~4.5 μm 波段区间平均截止透过率小于 0.3%; 3.5 μm~4.05 μm 及 4.7 μm~5.0 μm 波段的平均透过率大于 95%, 镀膜后的面型被有效控制在较小范围; 膜层具有较好的复杂环境适应性, 成功通过了 GJB 2485-95 中牢固性、高温、低温、湿热等环境试验考核。

关　键　词: 电子束蒸发法; 石英晶振监控法; 红外滤光片; 薄膜; 反演修正
中图分类号: O484　　**文献标志码:** A　　**doi:** 10.37188/CO.2022-0193

1　Introduction

With the development of infrared optoelectronic technology, the application field of passive photoelectric detection and imaging system based on target infrared radiation is becoming more and more extensive, and plays an important role in enhancing the dynamic perception of complex environments[1-2]. In order to obtain a clearer infrared target imaging, the acquired target signal should be modulated or filtered by various means to suppress the interference of background noise and improve the contrast of the image. And a considerable part of the interference noise is from the environmental background, such as atmospheric CO_2 radiation interference[3-5], whose radiation peak wavelength position is at 2.7 μm, 4.3 μm and 15 μm, of which the radiation coefficient value at 4.3 μm is the largest, which is one of the most serious radiation sources in the background noise of MWiR detection imaging. Therefore, in order to effectively suppress the interference of CO_2 radiation 4.3 μm on the infrared target signal, and then obtain clear and stable infrared target imaging, filtering optics need to be introduced in the original infrared optical system.

At present, the method commonly used at home and abroad is the short-wave infrared band-pass filter[6-7]. However, while the short-wave infrared band-pass filter effectively removes 4.3 μm CO_2 radiation interference, the useful signal light with wavelength greater than 4.3 μm will also be filtered out, resulting in the useful MWiR signal light in the wavelength range from 3.0 μm to 5.0 μm not being fully effective. Therefore, in recent years, notch filter (also called bandstop filter or minus filter) with high transmittance for most MWiR wavelengths light and effective cutoff for light in a specific wavelength range (stop band) has received a lot of attention from researchers[8-9]. For example, Wang S L *et al*..[10] from Xi'an Institute of Applied Optics prepared a dual-channel bandpass filter with excellent spectral performance by using the method of respectively designing a MWiR bandpass filter film and a MWiR minus filter on both sides of a single-crystal germanium substrate; meanwhile, it is pointed out that the variation of the evaporation angle of the coating material and the accumulation

of errors in the thickness of each layer were the main reasons for the difference between the test spectrum of the experimental film and the theoretical design spectrum. Based on the Rugate theory, Zhang B S *et al*.. from Institute of Lanzhou Physics[11] designed 3.8 μm single-wavelength minus filter and 1.315 μm and 3.8 μm dual-wavelength minus filter, but it is difficult to achieve because the film layer is relatively complicated[12]; Gao P *et al*..[12] proposed the fold-like design method for notch filter, and analyzed the effects of various design parameters on the spectra; Zhou Sh *et al*..[13] from Shanghai Institute of Technical Physics designed the minus filter system and the long wave cut-off film system on both sides of the Ge substrate respectively to form a bi-color filter containing two channels, 3.2 μm−3.8 μm and 4.9 μm−5.4 μm, respectively. In addition, according to the theory of equivalent refractive index, the researchers also proposed multi-film design methods[14] and thickness matching layer method[15-16], but there are certain limitations in practical engineering implementation[12].

Therefore, to address the current problem of difficult design and accurate preparation of MWiR notch filters, we firstly adopt the Needle random interpolation optimization method based on the $(4H/L)^n$ basic film system structure to achieve the optimal design of high-performance MWiR notch filters; secondly, by establishing a multilayer film growth error correction model, the cumulative thickness error in the coating process is effectively reduced to ensure the accurate preparation of MWiR notch filters; finally, the low surface profile regulation of the MWiR notch filter is achieved by using the pre-substrate surface profile method. In addition, the surface morphology and the applicability to complex environments of the obtained MWiR notch filters are evaluated.

2 Film system design and analysis

There are various transparent film materials that can be selected in the 3 μm~5 μm MWiR band, such as Ge, Al_2O_3, SiO, ZnS, YbF_3, and ZnSe. Due to the thickness of MWiR notch filter film is relatively thick, if the material ZnS, YbF_3 and/or ZnSe is used, a large stress will be generated with the increase of the film deposition thickness, which is very easy to produce damage such as cracking and delamination. Meanwhile, considering the maturity of the existing coating process, the mechanical properties of the film layer and its matching with substrate Ge, Ge and Al_2O_3 are finally selected as the high and low refractive index materials of the film structure of MWiR notch filter. The thin film preparation method uses the electron beam evaporation method. The starting background vacuum of 1.3×10^{-3} Pa was used for film deposition, and the background vacuum was gradually increased to ~ 6×10^{-4} Pa with the increase of coating time. The substrate surface was pre-cleaned for 5 min using an APS ion source before coating, and the deposition process parameters are shown in Table 1. The variation of optical constants (refractive index and extinction coefficient) of the obtained high and low refractive index films in the wavelength range of 2.0 μm~10.0 μm are shown in Fig. 1 (color online).

Tab. 1 Deposition parameters of thin film

表 1 薄膜沉积工艺参数

Thin film	Oxygen flow (sccm)	Growth temperature (°C)	Deposition rate (nm/s)	Electron beam (mA)
Ge	–	200	0.35	250
Al_2O_3	20	200	0.30	320

From Fig. 1(a), it can be seen that the optical constants (refractive index *n* and extinction coefficient *k*) of the prepared Ge films show a trend of first decreasing and then stabilizing with the increase of the examined wavelength in the range of 2.0 μm~10 μm band, specifically, the refractive index of the film layer material gradually decreases from ~4.31 to ~4.20 and stabilizes. The extinction coefficient *k* gradually decreases from ~0.005 to 0, and it shows good infrared transparency properties

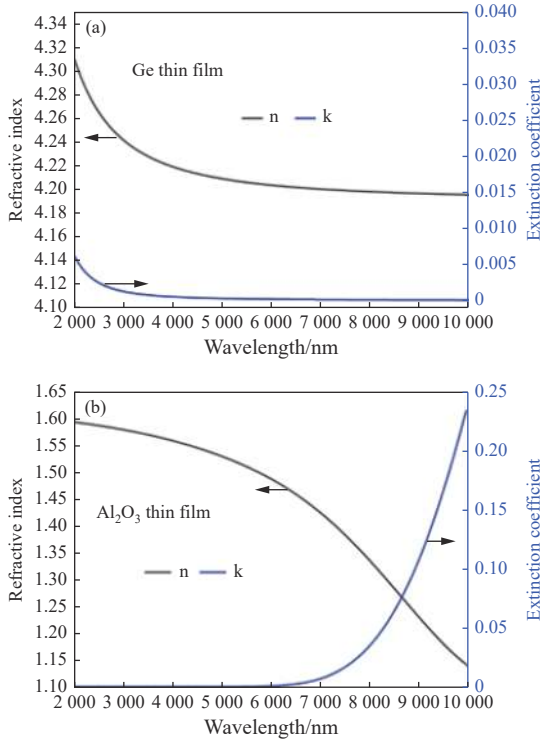

Fig. 1　Variation curves of refractive index and extinction coefficient of Ge and Al_2O_3 films

图 1　Ge 和 Al_2O_3 薄膜折射率和消光系数变化曲线

in the wavelength range of 3.5 μm~5.0 μm. For the prepared Al_2O_3 films, the variation of the optical constants is relatively more complicated due to the influence of the transparency band of the film material. As can be seen from Fig. 1(b), for the refractive index *n*, with the increase of the wavelength from 2 μm to 10 μm, the refractive index of the Al_2O_3 film material shows a gradual decreasing trend, and its average size is about 1.55 in the wave band of 3.5 μm~5 μm; the size of the extinction coefficient *k* shows an opposite trend, and is basically 0 in the band of 2.0 μm~6.0 μm, and the effect of the absorption loss of the film material is basically negligible; however, the value of *k* increases rapidly with the further increase of the wavelength.

During the optimized design of the MWiR notch filter film, the selected initial film system is Sub/(4H/L)^n/Air, where H is Ge and L is Al_2O_3, and after selecting the material and the initial film system, a 28-layer non-regular film system with relatively small thickness difference is obtained by using the Needle optimization algorithm in combination with multiple de-thinning and local re-optimization. The corresponding theoretical transmission spectral curves are shown in Fig. 2. From Fig. 2, it can be seen that the infrared notch filter film has good spectral characteristic. The average transmittance within the band ranges of 3.5 μm~4.05 μm and 4.7 μm~5.0 μm reaches ~97.21% and ~97.75%, respectively, and the average cut-off transmittance within the band of 4.2 μm~4.5 μm is ~0.27%. The total thickness of this MWiR notch filter film structure is ~18.6 μm, and it needs to be coated in three times to complete according to the existing coating process and crucible configuration, which puts higher requirements on the control precision and stability of the film preparation process.

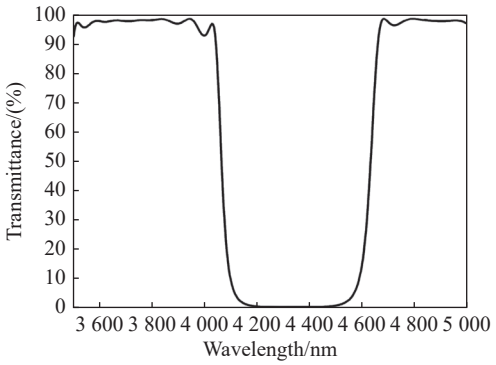

Fig. 2　Theoretical design spectral curve of MWiR notch filter

图 2　中波红外陷波滤光薄膜理论设计光谱曲线

The variation of the theoretical spectral transmittance of the MWiR notch filter film with the incident angle is shown in Fig. 3. As can be seen from Fig. 3, with the increase of the incident angle, the transmission spectra of the MWiR notch filter films gradually move toward the short-wave direction, and the cut-off transmittances at the wavelengths of 4.2 μm and 4.3 μm remain basically unchanged, both being lower than 0.5%, while the cut-off transmittance at the wavelength of 4.5 μm shows an increasing trend with the increase of the incident angle. At an incidence angle of 30°, the transmittance increases from 0.799% at vertical incidence to

32.17%. With the increase of incidence angle to 30°, the average transmittance within the band range of 3.5 μm~4.05 μm decreases rapidly, and the average transmittance within the band range of 4.7 μm~5.0 μm tends to increase and then decrease, which is related to the certain mismatch of the equivalent optical conductance of the film layer under the tilt angle incidence.

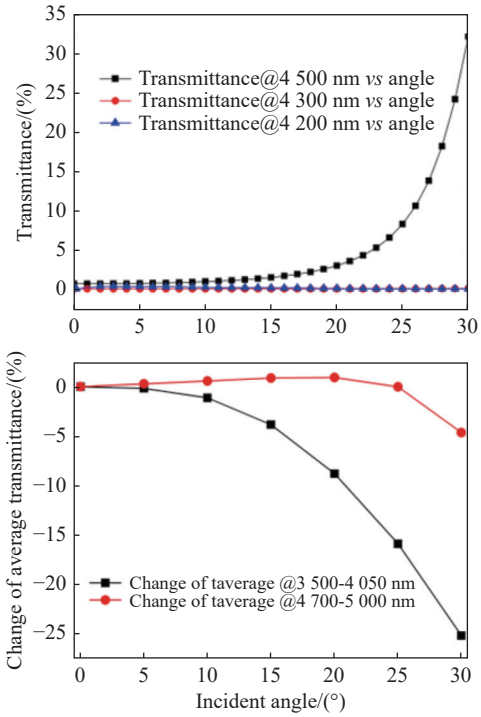

Fig. 3 Variation of theoretical spectral transmittance of films with incident angle

图 3 薄膜理论光谱透过率随入射角度的变化

3 Test results and analysis

3.1 Thin film inversion correction and spectral performance testing

During the coating process of MWiR notch filter film, due to the combined effect of various influencing factors (vacuum, evaporation state of the film material, monitoring errors, etc.), the actual thickness of the film layer will gradually deviate from the calibration value as the coating time increases by quartz crystal oscillator monitoring mode, which eventually causes the actual spectral curve to be significantly different from the theoretical design curve. Therefore, how to realize the accurate inversion and correction of the multilayer IR film is the key to the successful preparation of the IR notch filter.

To this end, a high standard and low refractive index film stack structure $(LH)^4L$ was grown and deposited by fixing the scaling factor in combination with the final optimized obtained multilayer film system structure, where the physical thickness of the high and low refractive index film layers in the $(LH)^4L$ standard film stack should be as close as possible to the average thickness of the high and low refractive index film layers in the film system structure, so as to reduce the influence of the difference in film thickness between the standard film stack and the actual film system structure on the final results. The curves of the theoretical design spectrum and the measured spectrum are shown in Fig. 4. As can be seen from Fig. 4, there is a large gap between the theoretical spectral curve distribution and the measured spectral curve within the investigated band range of 2.0 μm~6.0 μm, and the reasons for the deviation are closely related to various factors such as coating vacuum, crystal control monitoring error, temperature variation in the coating chamber and evaporation source state during the actual long time coating process.

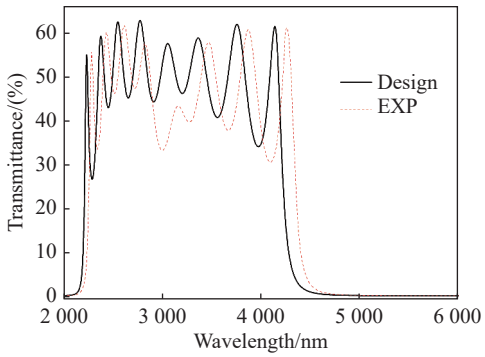

Fig. 4 Theoretical design and measured spectral curves of $(LH)^4L$ multilayer film structure under fixed scale factor

图 4 固定比例因子下，$(LH)^4L$ 多层薄膜结构理论设计与实测光谱曲线

Based on the measured spectral curves, the rel-

ative error distribution of the multilayer film structure was obtained by fitting with the software OplayerRe, as shown in Fig. 5. As can be seen from Fig. 5, with the increase of coating time, for the Al_2O_3 films with the low refractive index, the relative errors of the 1st, 3rd, 5th, 7th and 9th layers are 3.3%, 5.9%, 9.8%, 10.2% and 11.9%, respectively, and the amount of relative variation between the layers shows a trend of first increasing and then decreasing; for the Ge films with the high refractive index, the actual layer thickness is smaller than the designed layer thickness, and the relative error is negative, and varies between −2.7% and −1.7%, and the maximum relative variation between the film layers is 1.0%, which is within the theoretical fitting error range.

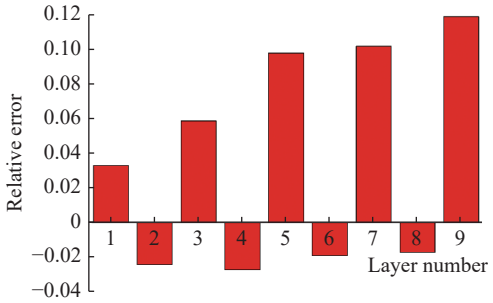

Fig. 5　Relative error distribution of each film

图 5　各膜层相对误差分布情况

With the above calibrated scale factors of high and low refractive index film thickness, the whole film structure of the MWiR notch filter film was prepared by electron beam evaporation method. During the preparation process, it is required to maintain the parameter consistency of each coating process, such as the starting coating vacuum, coating time, charge weight, and quartz crystal state. The designed and measured transmission spectra of the MWiR notch filter film are shown in Fig. 6. As can be seen from Fig. 6, the measured transmission spectra show a good consistency with the theoretical design spectra by using the modified film thickness gradient scaling factor, which further verifies the accuracy of the inverse fitting of the relative error of the above multilayer film.

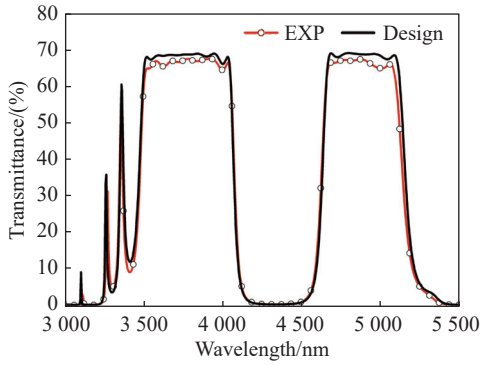

Fig. 6　Design and measured spectral curves of MWiR notch filter film obtained based on the modified scale factor

图 6　基于修正比例因子, 获得的中波红外陷波滤光薄膜设计与实测光谱曲线

Preparation of mid-wave infrared anti-reflective coating on the back of the MWiR notch filter is illustrated. The measured transmission spectra of the double-sided coating sample are shown in Fig. 7. As can be seen from Fig. 7, the average cut-off transmittance of MWiR notch filter film after double-sided coating is less than 0.3% in the band range of 4.2 μm~4.5 μm; the average transmittance is larger than 95% in the band range of 3.5 μm~4.05 μm and 4.7 μm~5.0 μm, which is about <2.0% lower than the theoretical design, but still higher than the technical index requirement of related products. The occurrence of this phenomenon is closely related to the increase of coating time, the oxidation of Ge material during the coating process, and the increase of surface roughness of deposited film layer.

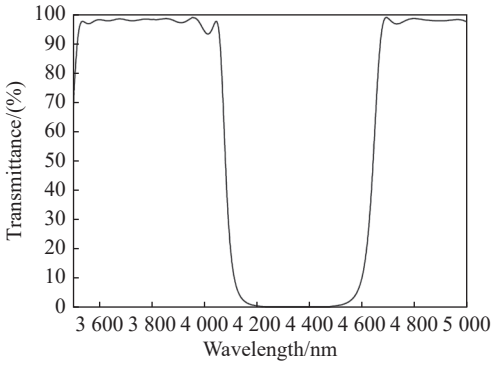

Fig. 7　Measured transmission spectrum curve after double-sided coating

图 7　双面镀膜后的实测透射光谱曲线

3.2 Film surface morphology

Fig. 8 (color online) shows the surface morphology of the MWiR notch filter coated on the germanium substrate. It can be also seen from Fig. 8 that the surface RMS values of the germanium substrate used before and after coating are 0.546 nm and 0.551 nm, respectively. In comparison, the surface roughness increases slightly after coating, which is related to the release of internal stresses in the film layer, structural defects in the film material, external contamination, and many other factors.

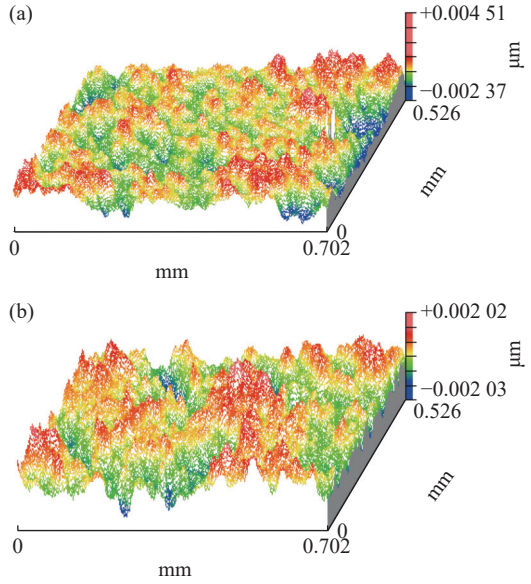

Fig. 8 Surface morphology graphs before (a) and after (b) coating

图 8 镀膜前 (a) 及镀膜后 (b) 表面形貌图

In addition, we also tested the change of reflective surface profile of the substrate before and after coating by ZYGO interferometer, as shown in Fig. 9 (color online). Wherein, Figs. 9(a)−9(b) show the changes of surface profile before and after coating without surface profile compensation, and Figs. 9(c)−9(d) show the changes of surface profile before and after coating with surface profile compensation. From Fig. 9(a) and Fig. 9(b), it can be seen that due to the thickness of the prepared MWiR notch filter film is thick, for the substrate with PV=0.121λ (where λ is at the test laser wavelength of 632.8 nm) before coating, it becomes 1.999λ after coating, which is far beyond the relevant usage requirements. In order to effectively reduce the surface profile change of the substrate after coating and avoid its influence on the wavefront, the method of presetting the surface profile of the substrate is introduced. As can be seen from Fig. 9(c) and Fig. 9(d), by presetting the 1.990λ surface profile state on the surface of the coated MWiR notch filter film, the surface profile becomes 0.191λ after coating, and the surface profile of the MWiR notch filter is improved more significantly.

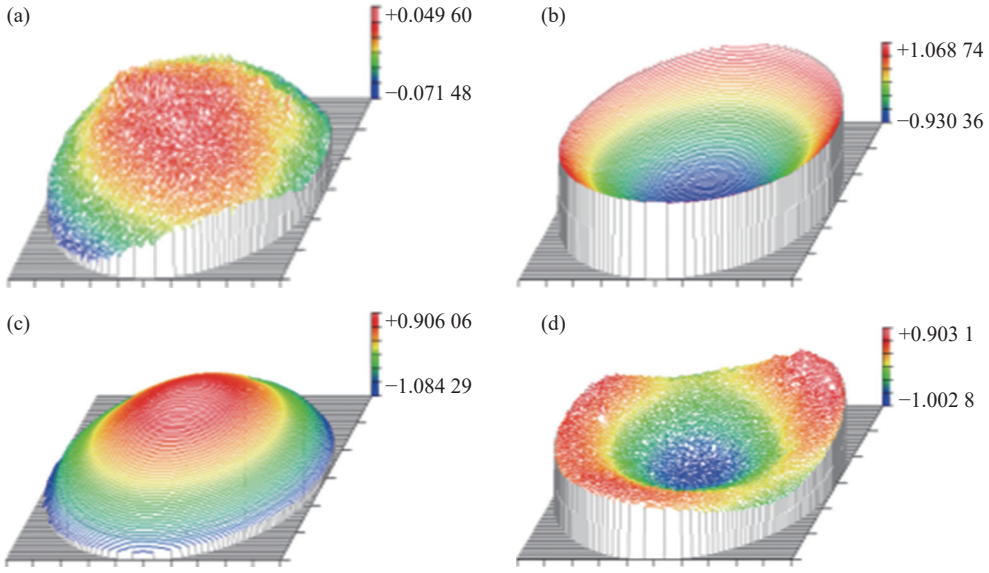

Fig. 9 Surface profile change before and after coating without surface profile compensation (a, b) and with surface profile compensation (c, d)

图 9 基底无面型补偿情况下，镀膜前后的面型变化 (a, b)；基底有面型补偿情况下，镀膜前后的面型变化 (c, d)

3.3　Film environmental adaptability

According to the environmental test requirements and methods of adhesion, high temperature, low temperature, humidity and heat in GJB2485~95 *General Specification for Optical Films*, the complex environmental adaptability assessment of MWiR notch filters was carried out systematically. The results show that after the environmental test, no cracking, delamination and other morphological features appear on the surface of the MWiR notch filter film, and the spectral transmission performance does not change significantly. It can be seen that the prepared MWiR notch filter film has excellent spectral performance and complex environmental adaptability.

4　Conclusion

In this paper, the design and development of 4.3 μm CO_2 radiation notch filter is realized based on Needle optimization algorithm, using electron beam evaporation method, combined with multilayer Ge/Al_2O_3 thin film growth error inversion correction model. The results show that the material correction scale factor of Al_2O_3 thin film tends to change regularly with the increase of coating time, which is related to various factors such as coating vacuum, evaporation state of film material, and monitoring error. The theoretical and experimental test results of the MWiR notch filter have good consistency, and its transmittance is less than 0.3% within the band range of 4.2 μm~4.5 μm, and its average transmittance is larger than 95% within the band ranges of 3.5 μm~4.05 μm and 4.7 μm~5.0 μm. The low surface profile (<0.2λ) modulation of the MWiR notch filters is successfully achieved by the pre-setting substrate surface profile method. The obtained MWiR notch filters have good environmental adaptability and successfully passed the environmental tests such as adhesion, high temperature, low temperature, humidity and heat in GJB 2485-95.

——中文对照版——

1　引　言

随着红外光电技术的发展，基于目标红外辐射的被动光电探测与成像系统应用愈加广泛，对于增强复杂环境动态感知能力发挥着重要作用[1-2]。为了获取更加清晰的红外目标成像，对于采集到的目标信号要利用多种手段进行调制或滤波，以抑制背景噪声干扰，提高图像对比度。而干扰噪声相当一部分来自环境背景，如大气 CO_2 辐射干扰[3-5]，其辐射峰波长位于 2.7 μm、4.3 μm 和 15 μm，其中 4.3 μm 处辐射系数值最大，是中波红外探测成像背景噪声中最严重的辐射源之一。因此，为了有效压制 4.3 μm CO_2辐射对红外目标信号的干扰，以获取清晰、稳定的红外目标成像，需在原有的红外光学系统中引入滤波光学器件。

目前，国内外普遍采用的方法是红外短波通滤光片[6-7]。然而，红外短波通滤光片在有效去除 4.3 μm CO_2 辐射干扰的同时，对于大于 4.3 μm 的部分有用信号光也会被一并滤除，致使 3.0 μm~5.0 μm 波长区间的中波红外有用信号光无法充分发挥作用。因此，近年来，对大部分中波红外波长光具有较高透过率，而对特定波长范围（阻带）内的光可实现有效截止的陷波滤光片（也称带阻滤光片或负滤光薄膜）受到了国内外学者的广泛关注[8-9]。例如：西安应用光学研究所王松林等[10]采用在单晶锗基底两面分别设计中波红外带通滤光膜和中波红外负滤光膜的方法，制备了一种光谱性能优良的双通道带通滤光片；同时其指出，镀膜材料蒸发角的变化和各层膜厚误差累积，是导致实验片测试光谱与理论设计光谱有差异的主要原因。兰州物理研究所的张佰森等[11]基于 Rugate 理论方法，设计了 3.8 μm 单波长负滤光薄膜和 1.315 μm、3.8 μm 双波长负滤光薄膜，但由于膜层相对较为复杂，实现难度较大[12]；高鹏等[12]提出了陷波滤光片的类褶皱设计方法，并分析了各设计参数对光谱的影响；周晟等[13]在 Ge 基片

两面分别设计了负滤光膜系和长波截止膜系，组合形成了包含 3.2 μm~3.8 μm 和 4.9 μm~5.4 μm 两个通道的双色滤光片。此外，依据等效折射率理论，研究人员还提出了多膜料设计方法[14]、厚度匹配层方法[15-16] 等，然而，这些方法在实际工程实现上均存在一定的局限性[12]。

针对目前中波红外陷波滤光片设计与精确制备难的问题，本文首先基于$(4H/L)^n$基本膜系结构，采用 Needle 随机插层优化方法，实现了高性能中波红外陷波滤光片的优化设计；其次，通过建立多层薄膜生长误差修正模型，有效降低了镀膜过程中存在的累积厚度误差影响，保证了中波红外陷波滤光片的精确制备；最后，采用预置基底面型方法，实现了中波红外陷波滤光片的低面型调控。此外，本文还对所获得的中波红外陷波滤光片进行了表面形貌以及复杂环境适用性考核与评价。

2 膜系设计与分析

在 3 μm~5 μm 中波红外波段区间可选择的透明薄膜材料有很多种，如 Ge、Al_2O_3、SiO、ZnS、YbF_3、ZnSe 等。由于中波红外陷波滤光薄膜相对较厚，若采用 ZnS、YbF_3、ZnSe 材料，随着膜层沉积厚度的增加，将产生较大的应力水平，极易产生开裂、脱膜等损伤；同时，综合考虑现有镀膜工艺成熟度、膜层机械性能及其与 Ge 材料的结合性能，最终选择 Ge、Al_2O_3 作为中波红外陷波滤光薄膜结构的高、低折射率膜层材料。薄膜制备采用电子束蒸发方法。薄膜沉积的起始本底真空度为 1.3×10^{-3}Pa，随着镀膜时间的增加，本底真空度逐渐提高至~6×10^{-4} Pa。镀膜前使用 APS 离子源对基底表面进行预清洗 5 min，沉积工艺参数如表 1 所示。所获得的高、低折射率薄膜在 2.0 μm~10.0 μm 波段范围内的光学常数（折射率和消光系数）变化如图 1（彩图见期刊电子版）所示。

由图 1(a)可知，在 2.0 μm~10.0 μm 波段范围内，随着波长的增加，所制备的 Ge 薄膜光学常数（折射率 n 和消光系数 k）呈先降低后趋于稳定的变化趋势，具体而言，膜层材料的折射率由~4.31 逐渐降低至~4.20，并趋于稳定；消光系数 k 大小由~0.005 逐渐降低为 0，其在 3.5 μm~5.0 μm 波段区间呈现出了较好的红外透明特性。对于所制备的 Al_2O_3 薄膜，受限于薄膜材料透明区间的影响，其光学常数的变化相对较为复杂。由图 1(b)可知，对于折射率 n 而言，随着考察波长从 2 μm 增加至 10 μm，Al_2O_3 薄膜材料的折射率呈逐渐降低趋势，其在 3.5 μm~5 μm 波段区间的平均大小约为 1.55；消光系数 k 呈相反的变化趋势，在 2.0 μm~6.0 μm 波段区间，大小基本为 0，膜层材料吸收损耗的影响基本可以忽略。但随着波长的进一步增加，k 值迅速增大。

中波红外陷波滤光薄膜优化设计过程中，选择初始膜系为 Sub/$(4H/L)^n$/Air，其中 H 为 Ge，L 为 Al_2O_3。在选定材料和初始膜系后，采用 Needle 优化算法，结合多次去薄层和局部再优化处理，最终优化获得了厚度差异相对较小的 28 层非规整膜系。其所对应的理论透射光谱曲线如图 2 所示。由图 2 可知，红外陷波滤光薄膜具有较好的光谱特性，3.5 μm~4.05 μm 和 4.7 μm~5.0 μm 波段范围的平均透过率分别约达 97.21%、97.75%，在 4.2 μm~4.5 μm 波段区间的平均截止透过率约为 0.27%。该中波红外陷波滤光薄膜结构总厚度约为 18.6 μm，根据现有的镀膜工艺及坩埚配置，需要分 3 次才能镀制完成，这就对膜层制备工艺控制精度和稳定性提出了更高要求。

中波红外陷波滤光薄膜理论光谱透过率随入射角度的变化如图 3 所示。由图 3 可知，随着入射角度的增加，中波红外陷波滤光薄膜的透射光谱曲线逐渐向短波方向移动，波长 4.2 μm 和 4.3 μm 的截止透射率基本保持不变，均低于 0.5%，4.5 μm 截止波长的透射率随着入射角度的增加呈现不断升高的变化趋势，在入射角度为 30°时，透过率由垂直入射下的 0.799% 增加至 32.17%。随着入射角度增加至 30°，3.5 μm~4.05 μm 波段范围的平均透过率迅速降低，4.7 μm~5.0 μm 波段范围的平均透过率呈先增加后降低的趋势，该现象的产生与倾斜角度入射情况下膜层等效光学导纳存在一定失配有关。

3 测试结果与分析

3.1 薄膜反演修正及光谱性能测试

中波红外陷波滤光薄膜镀制过程中，采用石英晶振监控方式，随着镀膜时间的增加，受多种影响因素的共同影响（真空度、膜料蒸发状态、监控

误差等), 膜层实际厚度会逐渐偏离标定值, 最终造成实际光谱曲线与理论设计曲线具有较大差异。因此, 如何实现多层红外薄膜的精确反演与修正则是该红外陷波滤光片能否成功制备的关键。

为此, 结合最终优化获得的多层膜系结构, 通过固定比例因子的方式, 生长沉积了标准高、低折射率膜堆结构 $(LH)^4L$, 其中, $(LH)^4L$ 标准膜堆中高、低折射率膜层的物理厚度要尽可能接近膜系结构中高、低折射率膜层的平均厚度, 以降低标准膜堆与实际膜系结构之间由于膜层厚度差异对最终结果的影响。理论设计光谱与实测光谱曲线如图 4 所示。由图 4 可知, 在所考察的 2.0 μm~6.0 μm 波段范围内, 理论光谱曲线分布与实测光谱曲线之间存在较大的差距, 而造成该偏差的原因与实际长时间镀膜过程中镀膜真空度、晶控监控误差、镀膜室内温度变化、蒸发源状态等多种因素密切相关。

基于实测光谱曲线, 采用 OplayerRe 软件, 拟合获得了多层薄膜结构相对误差分布情况, 如图 5 所示。由图 5 可知, 随着镀膜时间的增加, 对于低折射率 Al_2O_3 薄膜而言, 第 1、3、5、7、9 层的相对误差分别为 3.3%、5.9%、9.8%、10.2%、11.9%, 膜层之间的相对变化量呈现先增大后减小的趋势; 对于高折射率 Ge 薄膜, 实际膜层厚度小于设计膜层厚度, 其相对误差为负值, 相对误差变化处于−2.7%~−1.7% 之间, 膜层之间的最大相对变化量为 1.0%, 处于理论拟合误差范围之内。

根据以上所标定的高、低折射率薄膜厚度比例因子, 采用电子束蒸发方法, 完成了中波红外陷波滤光膜全膜系结构制备。在制备过程中要求每次镀膜工艺状态尽可能保持一致, 如起始镀膜真空度、镀膜时间、装料重量、石英晶振状态等。中波红外陷波滤光薄膜设计与实测透射光谱曲线如图 6 所示。由图 6 可知, 采用修正后的膜层厚度渐变比例因子, 实测透射光谱曲线与理论设计光谱曲线的变化趋势呈现出了较好的一致性, 这也进一步验证了以上多层薄膜相对误差反演拟合的准确性。

在中波红外陷波滤光薄膜基片背面镀制中波红外增透薄膜, 双面镀膜后的实测透射光谱曲线, 如图 7 所示。由图 7 可知, 在 4.2 μm~4.5 μm 波段区间, 双面镀膜后的中波红外陷波滤光薄膜平均截止透过率小于 0.3%; 3.5 μm~4.05 μm 及 4.7 μm~5.0 μm 波段的平均透过率大于 95%, 与理论设计相比, 约有 2.0% 的降低, 但仍高于相关产品的技术指标要求。而该现象的产生与随着镀膜时间的增加, 镀膜过程中 Ge 料被氧化、沉积膜层表面粗糙度增大等因素密切有关。

3.2　薄膜表面形貌

图 8(彩图见期刊电子版)为锗基底以及镀膜后的中波红外陷波滤光片表面形貌图。由图 8 可知, 镀膜前所用锗基底的表面 RMS 值大小为 0.546 nm, 镀膜后膜层表面 RMS 大小为 0.551 nm。相比而言, 镀膜后表面粗糙略有增加, 而这与膜层内应力的释放、膜层材料结构缺陷、外部污染等诸多因素有关。

此外, 本文还通过 ZYGO 干涉仪测试了镀膜前后基底表面反射面型大小的变化情况, 如图 9(彩图见期刊电子版)所示。其中图 9(a)、9(b)为基底无面型补偿情况下, 镀膜前后的面型变化; 图 9(c)、9(d)为基底有面型补偿情况下, 镀膜前后的面型变化。由图 9(a)和图 9(b)可知, 由于所制备的中波红外陷波滤光薄膜较厚, 对于镀膜前面型为 PV=0.121λ(其中 λ 为测试激光波长 632.8 nm)的基片, 镀膜后变为 1.999λ, 已远远超出相关使用要求。为了有效降低镀膜后基底的面型变化, 避免其对波前的影响, 引入预置基底面型的方法。由图 9(c)和图 9(d)可知, 通过在镀中波红外陷波滤光薄膜面预置 1.990λ 面型状态, 镀膜后的面型变为 0.191λ, 中波红外陷波滤光片的面型得到了较为显著的改善。

3.3　薄膜环境适应性

根据 GJB2485-95《光学薄膜通用规范》中有关附着力、高温、低温、湿热等环境试验要求及方法, 系统开展了中波红外陷波滤光片复杂环境适应性试验。试验结果表明: 环境试验后, 中波红外陷波滤光薄膜表面未出现开裂、脱膜、分层等情况; 光谱透射性能未发生显著改变。由此可见, 所制备的中波红外陷波滤光薄膜具有优异的光谱性能和复杂环境适应性。

4　结　论

本文基于 Needle 优化算法, 采用电子束蒸发

方法，结合多层 Ge/Al_2O_3 薄膜生长误差反演修正模型，实现了 4.3 μm CO_2 辐射陷波滤光片的设计与研制。研究结果表明：随着镀膜时间的增加，Al_2O_3 薄膜材料修正比例因子呈规律性变化趋势，而这与镀膜真空度、膜料蒸发状态、监控误差等多种因素有关；中波红外陷波滤光片理论与试验测试结果具有较好的一致性，其在 4.2 μm~4.5 μm 波段区间透过率小于 0.3%；3.5 μm~4.05 μm 及 4.7 μm~5.0 μm 波段的平均透过率小于 95%。通过预置基底面型方法，成功实现了中波红外陷波滤光片的低面型（<0.2λ）调控。所获得的中波红外陷波滤光片具有较好的环境适应性，成功通过了 GJB 2485-95 中附着力、高温、低温、湿热等环境试验考核。

References:

[1] 郭纲, 戴艳丽, 叶名兰. 光电成像制导技术发展及在导弹中的应用[J]. 红外与激光工程, 2007, 36(S1): 31-34.
GUO G, DAI Y L, YE M L. Photoelectric homing technology and its appliance in missile[J]. *Infrared and Laser Engineering*, 2007, 36(S1): 31-34. (in Chinese)

[2] 黄俊, 张正勇, 田省民. 机载对地光电探测设备现状及发展趋势研究[J]. 红外技术, 2018, 40(5): 412.
HUANG J, ZHANG ZH Y, TIAN SH M. Current status and development trend of airborne air to ground electro-optical detection equipment[J]. *Infrared Technology*, 2018, 40(5): 412. (in Chinese)

[3] 吴杰, 廖光, 毛宏霞, 等. 高超声速流场中CO_2的红外辐射研究[J]. 红外与激光工程, 2013, 42(5): 1113-1116.
WU J, LIAO G, MAO H X, *et al*.. IR radiation of CO_2 in hypersonic flow fields[J]. *Infrared and Laser Engineering*, 2013, 42(5): 1113-1116. (in Chinese)

[4] GARRISON M, OZAWA T, LEVIN D. An improved CO_2, H_2O and soot infrared radiation models for high temperature flows[C]. *36th AIAA Plasmadynamics and Lasers Conference*, AIAA, 2005: 4777.

[5] CHEN W, WANG ZH X, MA D H, *et al*.. Calculation and simulation of infrared radiation characteristics of non-uniform hot gas[J]. *Infrared and Laser Engineering*, 2010, 39(1): 17-21.

[6] 张建付, 杨崇民, 刘青龙, 等. 中波红外3μm~5μm宽带通滤光片的研制[J]. 应用光学, 2013, 34(4): 695-699.
ZHANG J F, YANG CH M, LIU Q L, *et al*.. Study and preparation of mid-wave infrared 3μm~5μm broad band pass filter[J]. *Journal of Applied Optics*, 2013, 34(4): 695-699. (in Chinese)

[7] 陈朝平, 师建涛, 郭芮, 等. 中红外带通滤光片的设计与制备[J]. 应用光学, 2012, 33(3): 595-598.
CHEN CH P, SHI J T, GUO R, *et al*.. Design and preparation of mid-infrared bandpass filter[J]. *Journal of Applied Optics*, 2012, 33(3): 595-598. (in Chinese)

[8] 林永昌, 卢维强. 光学薄膜原理[M]. 北京: 国防工业出版社, 1990.
LIN Y CH, LU W Q. *Optics of Thin Films*[M]. Beijing: National Defense Industry Press, 1990.

[9] FAHR S, ULBRICH C, KIRCHARTZ T, *et al*.. Rugate filter for light-trapping in solar cells[J]. *Optics Express*, 2008, 16(13): 9332-9343.

[10] 王松林, 米高园, 张建付, 等. 中波红外双通道带通滤光片的研制[J]. 激光与红外, 2017, 47(6): 740-744.
WANG S L, MI G Y, ZHANG J F, *et al*.. Study and preparation of mid-infrared dual channel band-pass filter[J]. *Laser & Infrared*, 2017, 47(6): 740-744. (in Chinese)

[11] 张佰森, 马勉军, 熊玉卿, 等. 基于Rugate理论的负滤光片设计研究[J]. 真空与低温, 2010, 16(4): 219-222,232.
ZHANG B S, MA M J, XIONG Y Q, *et al*.. Study of designing minus filters method based on Rugate theory[J]. *Vacuum & Cryogenics*, 2010, 16(4): 219-222,232. (in Chinese)

[12] 高鹏, 阴晓俊, 赵帅锋, 等. 陷波滤光片的类褶皱设计[J]. 光学仪器, 2013, 35(6): 82-90.
GAO P, YIN X J, ZHAO SH F, *et al*.. Notch filter designed by a quasi-Rugate method[J]. *Optical Instruments*, 2013, 35(6): 82-90. (in Chinese)

[13] 周晟, 王凯旋, 刘定权, 等. 3.2~3.8μm和4.9~5.4μm红外双色滤光片的研制[J]. 中国光学, 2021, 14(3): 536-543.
ZHOU SH, WANG K X, LIU D Q, *et al*.. Research on infrared dual-color filters with 3.2~3.8μm and 4.9~5.4μm bands[J]. *Chinese Optics*, 2021, 14(3): 536-543. (in Chinese)

[14] 蔡渊, 周晟, 刘定权, 等. 基于组合Fabry-Perot膜系的中波红外双色滤光片设计[J]. 光学学报, 2016, 36(2): 0222004.
CAI Y, ZHOU SH, LIU D Q, *et al*.. Design of dual-band-pass optical filter based on combination of Fabry-Perot coatings in mid-infrared band[J]. *Acta Optica Sinica*, 2016, 36(2): 0222004. (in Chinese)

[15] LAPPSCHIES M, GÖRTZ B, RISTAU D. Application of optical broadband monitoring to Quasi-Rugate filters by ion-beam sputtering[J]. *Applied Optics*, 2006, 45(7): 1502-1506.

[16] HENDRIX K D, HULSE C A, OCKENFUSS G J, *et al*.. Demonstration of narrowband notch and multi-notch filters[J]. *Proceedings of SPIE*, 2008, 7067: 706702.

Author Biographics:

Shang Peng (1986—), male, Heze city, Shandong province, Ph.D., Senior Engineer. He received his Ph.D. degree from the University of Chinese Academy of Sciences in 2015, mainly engaged in the research of special optical materials and optical thin film design, preparation and testing. E-mail: shangpeng163@163.com

尚　鹏(1986—), 男, 山东菏泽人, 博士, 高级工程师, 2015 年于中国科学院大学获得博士学位, 主要从事特种光学材料及光学薄膜设计、制备与测试方面的研究。E-mail: shangpeng163@163.com

Cao Bo (1983—), male, Siping city, Jilin province, B.S., Engineer, received his B.S. degree from Changchun University of Science and Technology in 2007, mainly engaged in the research of optoelectronic materials, optical processing, optical thin film and its engineering applications. E-mail: caobo@guojing-tech.com

曹　波(1983—), 男, 吉林四平人, 本科, 工程师, 2007 年于长春理工大学获学士学位, 主要从事光电材料、光学加工、光学薄膜及其工程应用方面的研究。E-mail: caobo@guojing-tech.com

Liu Hua-song (1980—), male, Fuxin city, Liaoning province, PhD, researcher, mainly engaged in design, preparation and characterization technology of the optical thin film, and optical thin film material physics. E-mail: liuhuasong@hotmail.com

刘华松(1980—), 男, 辽宁阜新人, 博士, 研究员, 主要从事光学薄膜设计、制备与表征技术, 光学薄膜材料物理方面研究。E-mail: liuhuasong@hotmail.com